Available online at www.sciencedirect.com
SCIENCE DIRECT®
Optics Communications 216 (2003) 55–63
OPTICS COMMUNICATIONS
www.elsevier.com/locate/optcom

Focusing of light through a stratified medium: a practical approach for computing microscope point spread functions. Part I: Conventional microscopy

Olivier Haeberlé *

Groupe LabEl – Laboratoire MIPS, Université de Haute-Alsace IUT Mulhouse, 61 Rue Albert Camus, F-68093 Mulhouse Cedex, France

Received 31 July 2002; accepted 21 November 2002

Abstract

We propose a method for microscope point spread function computation in which both design and actual acquisition parameters are explicitly introduced in the integrals describing the electromagnetic field in the focal region. This model therefore combines the ease of use of the Gibson and Lanni scalar approach with the accuracy of the Török and Varga method. We also compare some theoretical predictions of this model with those of a scalar model. In particular, the scalar model underestimates the point spread function size. This has practical application, for example when deconvolving microscope images or analyzing point spread functions. The method may also be used for confocal microscopy.

PACS: 07.60.Pb; 42.25.Fx; 42.30.Va

Keywords: Optical microscopy; Focusing; Point spread function; Vectorial theory

1. Introduction

The description of waves in focal regions has lead to numerous efforts by many authors ([1] and references therein). The computation of the point spread function of the optical microscope has generated intensive work to establish theoretical models of image formation [2–10], mainly because of applications in biological and material sciences.

A commonly used diffraction model for microscope objective is that of Gibson and Lanni [2]. It is based on scalar diffraction theory. One advantageous feature of this model is that it specifically introduces as parameters to compute the PSF the design conditions of use of the objective, as recommended by the manufacturer, and the actual acquisition conditions, when known by the user. It is also implemented in the XCOSM package [11]. This software from the Biomedical Computer Laboratory (Washington University, St. Louis, Missouri, USA) provides the implementation of several algorithms for deconvolving 3D images, as

* Fax: +33-3-89-337605.
E-mail address: o.haeberle@uha.fr (O. Haeberlé).

0030-4018/02/$ - see front matter
doi:10.1016/S0030-4018(02)02282-4

well as for computing point spread functions from optical and confocal microscopes. It runs on Unix workstations and PCs.

For high numerical aperture objectives, the extremal incident rays are impinging at large angles of incidence on the various interfaces separating the microscope objective from the specimen and as a consequence, vectorial theories of diffraction seem mandatory. Such electromagnetic models are indeed available [3–10]. They however are less directly usable by non-specialists, as practical acquisition conditions do not directly appear as computational parameters.

We propose a diffraction model for point spread function computation, which combines the advantage of the Gibson and Lanni model [12], namely the clear introduction of design and actual conditions, with the rigor of the integral representation of Török and Varga [10].

2. Gibson and Lanni model

Gibson and Lanni [2] modeled the point spread function (PSF) of an optical microscope objective using the scalar diffraction theory of light. Throughout this paper, we will only consider the intensity PSF as it corresponds to what one can easily measure with an optical microscope. The intensity PSF is then given by

$$\mathrm{PSF}(x,y,z) = \left| \int_0^1 J_0\left(ka\rho\sqrt{\frac{x^2+y^2}{z}}\right) \times \exp(\mathrm{i}W(\rho))\rho\,\mathrm{d}\rho \right|^2. \quad (1)$$

When the microscope objective is used under design conditions as recommended by the manufacturer, the phase term $W(\rho)$ reduces to a defocus term, and Eq. (1) simply represents the classical 3D Airy distribution [12]. When differences exist between the design conditions and the actual conditions, this distribution is deformed, which materializes the presence of aberrations.

To calculate $W(\rho)$, one considers the path difference between one optical ray entering the objective under design conditions and one entering the objective under the actual conditions. Fig. 1 describes the considered setup. The optical path difference is then given by

$$\mathrm{OPD} = [\mathrm{ABCD}] - [\mathrm{PQRS}]. \quad (2)$$

One has to compute OPD with respect to the following quantities: θ is the angle of propagation of both rays entering the frontal lens of the objective; t_s the depth of the specimen under the cover glass; n_s the index of refraction of the specimen; t_g the thickness of the cover glass; n_g the index of refraction of the cover glass; t_i the thickness of the immersion medium layer; n_i the index of refraction of the immersion medium; and n is the index of refraction of the objective front lens.

The parameters with an asterisk * are values for the design conditions of use of the objective, those without an asterisk are the actual ones. Taking into account the Snell–Descarte law of refraction and the fact that the microscope obeys the Abbe sine condition, Gibson and Lanni propose for the computation of the OPD:

$$\mathrm{OPD} = \mathrm{OPD}_g + \mathrm{OPD}_i + \mathrm{OPD}_s. \quad (3)$$

The term OPD_g represents the aberration term due to the use of an improper cover glass (index of refraction or thickness differing from the design values)

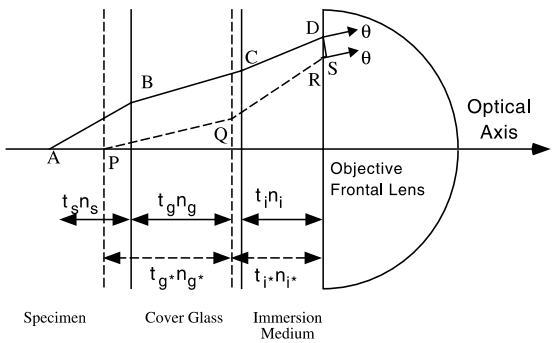

Fig. 1. Optical rays entering the frontal lens of a microscope objective in the Gibson and Lanni model in design conditions (dashed line) and actual conditions (solid line). The optical path difference to be computed is given by OPD = [ABCD] – [PQRS].

$$\mathrm{OPD_g} = n_\mathrm{g} t_\mathrm{g} \sqrt{1 - \left(\frac{n \sin\theta}{n_\mathrm{g}}\right)^2} - n_\mathrm{g}^* t_\mathrm{g}^* \sqrt{1 - \left(\frac{n \sin\theta}{n_\mathrm{gi}^*}\right)^2}. \quad (4)$$

The aberrations possibly induced by an incorrect immersion medium are given by

$$\mathrm{OPD_i} = n_\mathrm{i} t_\mathrm{i} \sqrt{1 - \left(\frac{n \sin\theta}{n_\mathrm{i}}\right)^2} - n_\mathrm{i}^* t_\mathrm{i}^* \sqrt{1 - \left(\frac{n \sin\theta}{n_\mathrm{i}^*}\right)^2}. \quad (5)$$

The specimen lying at depth t_s, under the coverslip, one has the supplemental term

$$\mathrm{OPD_s} = n_\mathrm{s} t_\mathrm{s} \sqrt{1 - \left(\frac{n \sin\theta}{n_\mathrm{s}}\right)^2}. \quad (6)$$

The computation of the intensity PSF described by Eq. (1) is then performed by computing the various terms (Eqs. (3)–(6)) with

$$W(\rho) = k\mathrm{OPD} \quad \text{and} \quad \rho = n \sin\theta / \mathrm{NA}. \quad (7)$$

This model is very convenient for computing PSFs in the sense that design and actual conditions of acquisition directly appear as input parameters (see Appendix A). It however suffers from several limitations.

First the apodizing function $a(\theta) = (\cos\theta)^{1/2}$ for an aberration free aplanetic system obeying the sine condition is not included in Eq. (1).

Secondly, for a high numerical aperture objective, the extremal incident rays are impinging at large angles of incidence on the two interfaces (immersion medium to cover glass, and cover glass to specimen) separating the microscope objective from the specimen. Even if one considers randomly or circularly polarized light, which would have for effect of averaging the various polarization contributions, these extremal rays are considered to be transmitted without reflections, namely with constant intensity, an assumption which may be questionable for high incidence rays or when large differences exist in the refraction indices.

As a consequence, one can question the accuracy of the predictions by this model. Even if "Gibson and Lanni demonstrated good agreements between their numerical results and experimental measurements of the aberrated point spread function. This and some other theories confirm that, while it is essential to construct mathematically rigorous theories, it is sometimes possible to obtain accurate predictions using approximate physical models based on wave optics" (from [13]), the recent progress in instrumentation (compared to the experiments described in [2]) should permit to better compare experimental data with computations from this scalar model and from a vectorial model.

3. Török and Varga model

An elegant description of high numerical aperture focusing of electromagnetic waves is that of Wolf [3,4], who proposed a formalism based on the angular spectrum of plane waves, from which integral formulas are obtained. This formulation was later on subsequently generalized by Török et al. [6–8] who considered the focusing of an electromagnetic wave through a planar interface separating materials with mismatched indices of refraction. Finally, a further extension of this method describes electromagnetic waves focused through a stratified medium [10]. We recall here briefly the main results, using the same notation as in [10].

One considers a linearly polarized (along the x-axis) monochromatic wave focused through a three-layer medium (see Fig. 2). The origin of the (x, y, z) coordinate system is at the Gaussian focus point. The intensity illumination PSF at point $P(x, y, z)$ can then be computed as

$$\mathrm{PSF}(x, y, z) = |\mathbf{E}|^2 = \left|\mathbf{E}_{3x} + \mathbf{E}_{3y} + \mathbf{E}_{3z}\right|^2, \quad (8)$$

the components being given by (with ϕ in spherical polar coordinates)

$$\begin{aligned} E_{3x} &= -\mathrm{i}(I_{0\,\mathrm{ill}} + I_{2\,\mathrm{ill}} \cos 2\phi), \\ E_{3y} &= -\mathrm{i}(I_{2\,\mathrm{ill}} \sin 2\phi), \\ E_{3z} &= -2 I_{1\,\mathrm{ill}} \cos\phi, \end{aligned} \quad (9)$$

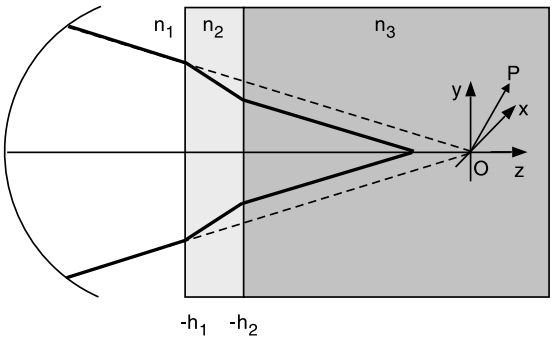

Fig. 2. Diagram showing an electromagnetic wave focused by a lens through a three-layer stratified medium in the Török and Varga approach. The origin O of the (x, y, z) reference frame is at the unaberrated Gaussian focus point.

$$
\begin{aligned}
I_{0\mathrm{ill}} &= \int_0^{\alpha} \sqrt{\cos\theta_1}\sin\theta_1 J_0(k_1(x^2+y^2)^{1/2}\sin\theta_1) \\
&\quad \times (T_{2s}+T_{2p}\cos\theta_3)\exp(\mathrm{i}k_0\Psi_{\mathrm{i}}) \\
&\quad \times \exp(\mathrm{i}k_3 z\cos\theta_3)\mathrm{d}\theta_1, \\
I_{1\mathrm{ill}} &= \int_0^{\alpha} \sqrt{\cos\theta_1}\sin\theta_1 J_1(k_1(x^2+y^2)^{1/2}\sin\theta_1) \\
&\quad \times T_{2p}\sin\theta_3\exp(\mathrm{i}k_0\Psi_{\mathrm{i}}) \\
&\quad \times \exp(\mathrm{i}k_3 z\cos\theta_3)\mathrm{d}\theta_1, \\
I_{2\mathrm{ill}} &= \int_0^{\alpha} \sqrt{\cos\theta_1}\sin\theta_1 J_2(k_1(x^2+y^2)^{1/2}\sin\theta_1) \\
&\quad \times (T_{2s}-T_{2p}\cos\theta_3)\exp(\mathrm{i}k_0\Psi_{\mathrm{i}}) \\
&\quad \times \exp(\mathrm{i}k_3 z\cos\theta_3)\mathrm{d}\theta_1.
\end{aligned}
\tag{10}
$$

The so-called initial aberration function [10] is given by

$$
\Psi_{\mathrm{i}} = h_2 n_3\cos\theta_3 - h_1 n_1\cos\theta_1. \tag{11}
$$

The transmission coefficient for a three-layer medium is given by

$$
T_{2s,p} = \frac{t_{12s,p}t_{23s,p}\exp(\mathrm{i}\beta)}{1 + r_{12s,p}r_{23s,p}\exp(2\mathrm{i}\beta)} \tag{12}
$$

with $\beta = k_2|h_2 - h_1|\cos\theta_2$ [14] and the Fresnel coefficients for transmission and reflection being given by

$$
\begin{aligned}
t_{nn+1,s} &= \frac{2n_n\cos\theta_n}{n_n\cos\theta_n + n_{n+1}\cos\theta_{n+1}}, \\
t_{nn+1,p} &= \frac{2n_n\cos\theta_n}{n_{n+1}\cos\theta_n + n_n\cos\theta_{n+1}}, \\
r_{nn+1,s} &= \frac{n_n\cos\theta_n - n_{n+1}\cos\theta_{n+1}}{n_n\cos\theta_n + n_{n+1}\cos\theta_{n+1}}, \\
r_{nn+1,p} &= \frac{n_{n+1}\cos\theta_n - n_n\cos\theta_{n+1}}{n_{n+1}\cos\theta_n + n_n\cos\theta_{n+1}}.
\end{aligned}
\tag{13}
$$

This vectorial model has been shown to be compatible with the Huygens–Fresnel approach [9] of diffraction in the case of a two-layer medium (when $n_2 = n_3$ for example). It has been successfully used to compute the PSF of an optical microscope and to show how adapting the cover glass thickness permits to compensate the spherical aberration introduced by immersion medium and specimen refractive indices mismatch [10]. It has also permitted to study aberration correction using a Zernike expansion of the aberration function [15].

We will now show how one can combine the above approach with the ease of use of the Gibson and Lanni model.

4. Discussion

In biological microscopy, three cases are commonly to be considered: dry objectives, oil immersion objectives and water immersion objectives. As pointed out by Török and Varga [10], for such layers the Fresnel reflection coefficients $r_{s,p}$ given by Eq. (13) are much smaller than unity. The denominator of $T_{2s,p}$ can therefore be considered as unity. As a consequence, the overall aberration function for a three-layer medium can be written as

$$
\Psi = \sum_{j=1}^{3} h_j(n_{j+1}\cos\theta_{j+1} - n_j\cos\theta_j). \tag{14}
$$

If the numerical aperture of the illuminating objective is limited such that there is no non-ordinary refraction at both interfaces, Eq. (14) may be rewritten with Gibson and Lanni notations ($\rho = n_1\sin\theta_1/\mathrm{NA}$, $n_1\sin\alpha = \mathrm{NA}$, $n_3 = n_{\mathrm{s}}$, $n_2 = n_{\mathrm{g}}$, $h_2 = t_{\mathrm{s}}$ and $h_1 = t_{\mathrm{s}} + t_{\mathrm{g}}$) as

$$\Psi = -(t_s + t_g)n_i\sqrt{1 - \left(\frac{NA\rho}{n_i}\right)^2} + n_s t_s\sqrt{1 - \left(\frac{NA\rho}{n_s}\right)^2} + n_g t_g\sqrt{1 - \left(\frac{NA\rho}{n_g}\right)^2}. \quad (15)$$

Comparing Eq. (15) with Eq. (4)–(7) highlights the parallel, which exists between both methods. The second term of the above equation represents the aberration introduced by the focalization of the wave at depth ($h_2 = t_s$) under the second nterface, namely under the cover glass. It is identical to the term given by Eq. (6). The third term represents the aberration introduced by the cover glass. It is identical to the first term of Eq. (4), the second term of Eq. (4) being introduced has a compensation from the objective to express that when a design (thickness and refraction index) cover glass is used, its aberration cancels with that introduced by the objective.

The first term is to be split into two

$$\Psi_i = \Psi_{i1} + \Psi_{i2} = -t_g n_i\sqrt{1 - \left(\frac{NA\rho}{n_i}\right)^2} - t_s n_i\sqrt{1 - \left(\frac{NA\rho}{n_i}\right)^2}. \quad (16)$$

Eq. (16) represents the so-called initial aberration function [10]. The first term of Eq. (16) only depends on ρ and not on the specimen depth. So to correct this initial spherical aberration, one has also to compensate for that term. This is done by saying that the objective will introduce an aberration given by

$$\Psi_{obj} = +t_{g^*} n_{i^*}\sqrt{1 - \left(\frac{NA\rho}{n_{i^*}}\right)^2} \quad (17)$$

so that when a design thickness cover glass is used in conjunction with a design immersion medium refractive index, these phase factors compensate.

Török and Varga [10] consider the focusing of a wave into the medium at a certain depth under the cover glass, which explains the presence of the term Ψ_{i2} in Eq. (16), which does not appear in Eqs. (4)–(7). In the Gibson and Lanni model [2], one considers on the contrary a scan of a point like source to acquire a 3D PSF. As a consequence, the immersion medium layer thickness changes during the scan. If one expresses this change as a function of the defocus, one obtains

$$t_i = n_i\left[\frac{z}{n_i} + \left(\frac{t_{g^*}}{n_{g^*}} - \frac{t_g}{n_g}\right) + \left(\frac{t_{i^*}}{n_{i^*}} - \frac{t_s}{n_s}\right)\right]. \quad (18)$$

Inserting Eq. (18) into Eq. (5), one obtains for the optical path difference the final expression

$$\begin{aligned} OPD = {} & n_i z\sqrt{1 - \left(\frac{NA\rho}{n_i}\right)^2} \\ & + n_g t_g\left(\sqrt{1 - \left(\frac{NA\rho}{n_g}\right)^2} - \left(\frac{n_i}{n_g}\right)^2\sqrt{1 - \left(\frac{NA\rho}{n_i}\right)^2}\right) \\ & - n_g^* t_g^*\left(\sqrt{1 - \left(\frac{NA\rho}{n_g^*}\right)^2} - \left(\frac{n_i}{n_g^*}\right)^2\sqrt{1 - \left(\frac{NA\rho}{n_i}\right)^2}\right) \\ & - n_i^* t_i^*\left(\sqrt{1 - \left(\frac{NA\rho}{n_i^*}\right)^2} - \left(\frac{n_i}{n_i^*}\right)^2\sqrt{1 - \left(\frac{NA\rho}{n_i}\right)^2}\right) \\ & - n_s t_s\left(\sqrt{1 - \left(\frac{NA\rho}{n_s}\right)^2} - \left(\frac{n_i}{n_s}\right)^2\sqrt{1 - \left(\frac{NA\rho}{n_i}\right)^2}\right). \end{aligned} \quad (19)$$

We recognize in the first term of Eq. (19) the term Ψ_{i2} of Eq. (16), which proves that in fact the Gibson and Lanni approach of calculating the

optical path difference, including terms relative to the thickness and index of refraction of the immersion layer is indeed equivalent to the Török and Varga approach. As a consequence, we propose to combine the integral equations of Török and Varga with the Gibson and Lanni method for computing the phase difference, so that Eqs. (8) and (9) are to be calculated with Eqs. (4)–(6) and with

$$
\begin{aligned}
I_{0\,\mathrm{ill}} &= \int_0^{\alpha} \sqrt{\cos\theta_1}\sin\theta_1 J_0(k_1(x^2+y^2)^{1/2}\sin\theta_1)\\
&\quad\times (t_{12s}t_{23s} + t_{12p}t_{23p}\cos\theta_3)\\
&\quad\times \exp(\mathrm{i}k_0\mathrm{OPD})\mathrm{d}\theta_1,\\
I_{1\,\mathrm{ill}} &= \int_0^{\alpha} \sqrt{\cos\theta_1}\sin\theta_1 J_1(k_1(x^2+y^2)^{1/2}\sin\theta_1)\\
&\quad\times (t_{12p}t_{23p}\sin\theta_3)\\
&\quad\times \exp(\mathrm{i}k_0\mathrm{OPD})\mathrm{d}\theta_1,\\
I_{2\,\mathrm{ill}} &= \int_0^{\alpha} \sqrt{\cos\theta_1}\sin\theta_1 J_2(k_1(x^2+y^2)^{1/2}\sin\theta_1)\\
&\quad\times (t_{12s}t_{23s} - t_{12p}t_{23p}\cos\theta_3)\\
&\quad\times \exp(\mathrm{i}k_0\mathrm{OPD})\mathrm{d}\theta_1.
\end{aligned}
\tag{20}
$$

5. Numerical results

Fig. 3 shows point spread functions computed at $\lambda = 488$ nm and using Eq. (20) for an air immersion ($n_{i^*} = 1$) objective of numerical aperture 0.9, designed to be used with a cover glass of index $n_{g^*} = 1.54$ and thickness $t_{g^*} = 170$ μm and at a depth of 50 μm below the cover glass in a watery medium $n_s = 1.33$. The actual cover glass thickness is: (a) 120, (b) 170 and (c) 220 μm with all other actual parameters having their design values. (Appendix A shows the various parameters used in the Gibson and Lanni approach.)

These curves are identical to those published in [10] (Fig. 4(b)), which have been computed with Eq. (10) and introducing the correction for a 170 μm cover glass. The sole difference is that when using Eq. (20) with the Gibson and Lanni parameters, one computes the PSF in an absolute reference frame centered at the geometrical position of the focal point, while curves presented in

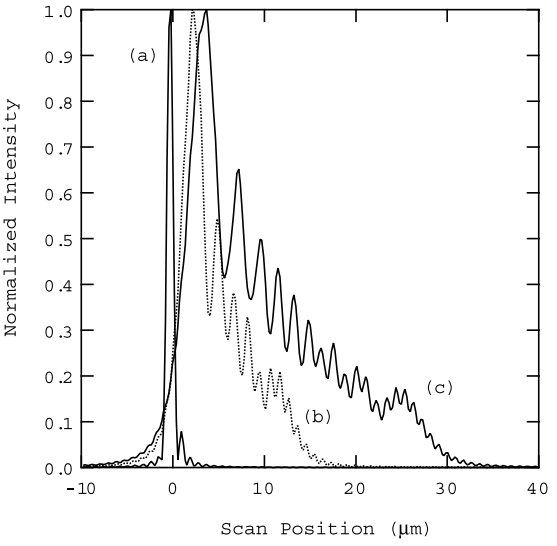

Fig. 3. Optical axis profile of the point spread function for an air immersion ($n_i = n_{i^*} = 1$) objective of numerical aperture NA = 0.9 imaging at $\lambda = 488$ nm a specimen at a depth of 50 μm in a watery medium ($n_s = 1.33$) through a cover glass ($n_g = n_{g^*} = 1.54$, $t_{g^*} = 170$ μm) of thickness 120 μm (curve a), 170 μm (curve b) and 220 μm (curve c).

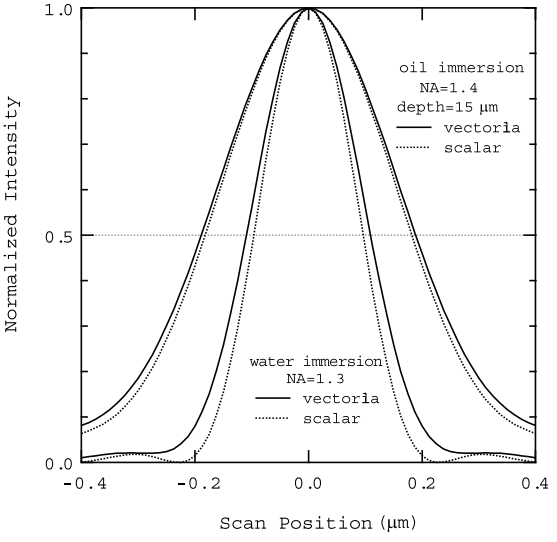

Fig. 4. Lateral profile of the point spread function at $\lambda = 488$ nm for a water immersion objective with NA = 1.3 (all parameters satisfying the design conditions) and an oil immersion objective with NA = 1.4 and with a specimen depth of 15 μm. Dashed curves: scalar model. Solid curves: vectorial model with unpolarized radiation.

[10] are displayed with the distance of the last interface from the unaberrated Gaussian focus as horizontal axis. We also computed these curves using Eq. (12) without approximation on the Fresnel reflection coefficients $r_{s,p}$ given by Eq. (13). The difference is below 1%, which justifies the approximation made by Török and Varga to obtain Eq. (14), and as a consequence also validates the equivalence with the Gibson and Lanni approach we highlighted.

In Fig. 4, we show the lateral PSF profile for a water immersion objective ($n_i = 1.33$) with NA = 1.3 imaging in a watery medium ($n_s = 1.33$) and for an oil immersion objective ($n_i = 1.515$) with NA = 1.4 imaging in a watery medium ($n_s = 1.33$) at a depth of 15 μm. The dashed curves are computed with the Gibson and Lanni model and the solid curves with our method. In both case, all actual parameters satisfy the design conditions. A random emission of light at $\lambda = 488$ nm is considered so that the ϕ dependence in Eq. (9) disappears [5,6]. Fig. 4 shows that the resolution (measured at FWHM of the distribution) is in fact overestimated (by 14%) when using a scalar model for the water immersion objective. This has consequence when deconvolving data from a fluorescence microscope: as the scalar model underestimates the actual PSF size, measurement on objects with extension similar to the objective resolution will result in an overestimation of the actual object size. Also, when analyzing an experimental PSF [16], the use of a scalar model may lead to an underestimation of the actual numerical aperture.

For a NA = 1.4 oil immersion objective, the lateral size difference is 15% when the specimen is placed just below the cover glass. One could argue that when using the same NA = 1.4 objective to image a specimen at a depth of 15 μm, the error on the lateral resolution is only 4% (Fig. 4). However the loss in resolution is such that using a water immersion objective would give a better resolution despite the lower NA. These results confirm the statement by Sheppard and Török suggesting that "use of high aperture scalar theory is not particularly useful as an approximation to the vectorial case" [17], at least when there is no aberration, and show that it is indeed necessary to use a vectorial model when precise quantitative measurements are to be done after a deconvolution if using a high NA objective. Note that a scalar model may give results with the desired accuracy for lower NA objectives: the error on the lateral resolution is below 3% for NA = 0.8.

Finally, the similarity between Eq. (1) and Eq. (20) shows that only little modifications of the XCOSM code may permit to merge the ease of use of this software with the more accurate model of Török and Varga, therefore facilitating its adoption by non-specialists in optics.

6. Application to confocal and multiphoton microscopy

Confocal [18] and multiphoton [19] microscopy are widely used for 3D investigations of biological structures because of their inherent optical sectioning capabilities and deeper penetration depth. Theoretical treatments of confocal fluorescence microscopy have been presented by several authors [20–22]. These models are based on the high-angle vectorial diffraction integrals proposed by Richards and Wolf [3,4]. Assuming that the fluorescent particle acts as a perfectly isotropic radiator, one shows that the confocal microscope PSF is obtained by multiplying the illumination PSF by the detection PSF. For multiphoton microscopy, the probability of excitation of the dipole is proportional to the intensity of the illumination to the power of the order of the multiphoton process. Fluorescence is however known to be generally polarized, and dipole emission models better the fluorescence process than isotropic radiation. However, models used to describe the image formation process in confocal and multiphoton microscopy and considering dipole emission assume that the dipole is located in a homogeneous medium [23–26]. This assumption may be fulfilled for example when using a water immersion objective working without cover glass. A rigorous treatment of dipole imaging through dielectric interfaces remains to be proposed. Ref. [27] sets up the basis of such a theory.

However, when the fluorescent molecule can freely rotate between excitation and emission, for unpolarized or circularly polarized illumination and detection, and as long exposure time (com-

pared to fluorescence life-time) is required, the image is obtained by averaging over all dipole orientations. In that case, one finds that the PSF of a confocal microscope observing dipoles is the same as if an isotropic radiator is considered [23]

$$\mathrm{PSF}_{\mathrm{conf}}(x,y,z) = \left(|I_{0\,\mathrm{ill}}|^2 + 2|I_{1\,\mathrm{ill}}|^2 + |I_{2\,\mathrm{ill}}|^2\right) \times \left(|I_{0\,\mathrm{det}}|^2 + 2|I_{1\,\mathrm{det}}|^2 + |I_{2\,\mathrm{det}}|^2\right). \tag{21}$$

The diffraction integrals are computed at the illumination and detection wavelengths and for finite size pinhole, a convolution with the pinhole aperture is necessary (note that in the XCOSM implementation of this model, illumination and detection PSFs are computed at the same observation wavelength, which constitutes another approximation).

Under this assumption of freely rotating fluorescent molecules, our model given by Eq. (20) may also be used to compute confocal and multiphoton PSFs. We would like to emphasize one obvious limitation of this approach. Fresnel coefficients differ when for example propagation occurs from oil to glass or from glass to oil. So, for focusing through a layered medium, the illumination and detection PSFs should be slightly different even if computed at the same wavelength. We believe the difference is very small for water or oil immersion objectives, and we will assume the detection PSF may be computed as the illumination PSF using Eq. (20). This approximation may however fail for air immersion objectives, because of the large difference in the refractive indexes.

7. Conclusion

We have shown how the approach of Gibson and Lanni to calculate the phase difference between optical rays in actual and design conditions of use of a microscope objective can be combined with the vectorial model of Török and Varga. One then obtains a convenient model to precisely compute the point spread function of a microscope objective, which explicitly introduces experimental and design acquisition parameters. Comparing simulations of the scalar model with ours shows that for high NA objectives, noticeable differences appear. For precise deconvolution results and quantitative measurements, use of a vectorial model is therefore mandatory. Our approach may also be used to compute point spread functions for confocal microscopy, under some assumptions relative to the fluorescent dye.

Acknowledgements

The author would like to gratefully acknowledge Peter Török for valuable discussions about his work.

Appendix A

List of the parameters of the XCOSM package to compute the PSF of an optical microscope:

Nxy: 128	size of the image in x and y
deltaxy: 0.068	pixel size in image space in μm
Nz: 128	size of the image in z (optical axis)
deltaz: 0.1	pixel size in z in μm
mag: 100	lateral magnification
NA: 0.9	numerical aperture of the objective
workdist: 0.16	working distance of the objective in mm
lamda: 0.000488	fluorescence wavelength in mm
slipdesri: 1.525	cover glass design refractive index
slipactri: 1.525	cover glass actual refractive index
slipdesth: 0.170	cover glass design thickness in mm
slipactth: 0.120	cover glass actual thickness in mm
medesri: 1	immersion medium design refractive index
medactri: 1	immersion medium actual refractive index
specri: 1.33	specimen refractive index
specthick: 0.050	specimen depth in mm
desot: 160	design tube length in mm
actot: 160	actual tube length in mm

(Note that in a modern, infinity-corrected microscope, the two last parameters are meaningless.)

References

[1] J.J. Stamnes, Waves in Focal Regions, first ed., Adam Hilger, Bristol, UK, 1986.
[2] S.F. Gibson, F. Lanni, J. Opt. Soc. Am. A 8 (1991) 1601.
[3] E. Wolf, Proc. R. Soc. London, Ser. A 253 (1959) 349.
[4] B. Richards, E. Wolf, Proc. R. Soc. London, Ser. A 253 (1959) 358.
[5] S.W. Hell, G. Reiner, C. Cremer, E.H.K. Stelzer, J. Microsc. (Oxford) 169 (1993) 391.
[6] P. Török, P. Varga, Z. Laczik, G.R. Booker, J. Opt. Soc. Am. A 12 (1995) 325.
[7] P. Török, P. Varga, G.R. Booker, J. Opt. Soc. Am. A 12 (1995) 2136.
[8] P. Török, P. Varga, A. Konkol, G.R. Booker, J. Opt. Soc. Am. A 13 (1996) 2232.
[9] A. Egner, S.W. Hell, J. Microsc. (Oxford) 193 (1999) 244.
[10] P. Török, P. Varga, Appl. Opt. 36 (1997) 2305.
[11] http://3Dmicroscopy.wustl.edu/~xcosm.
[12] M. Born, E. Wolf, Principles of Optics, sixth ed., Pergamon, London, 1991.
[13] P. Török, S.J. Hewlett, P. Varga, J. Microsc. (Oxford) 188 (1997) 158.
[14] In Refs. [10] and [15], a factor 2 has been inadvertently introduced in the definition of β.
[15] P. Török, Optical Memory and Neural Networks 8 (1999) 9.
[16] O. Haeberlé et al., Opt. Commun. 196 (2001) 109.
[17] C.J.R. Sheppard, P. Török, Optik 105 (1997) 77.
[18] M. Minsky, Scanning 10 (1988) 128.
[19] W. Denk, J.H. Strickler, W.W. Webb, Science 248 (1990) 73.
[20] H.T.M. van der Voort, G.J. Brakenhoff, J. Microsc. (Oxford) 158 (1990) 43.
[21] S.W. Hell, E.H.K. Stelzer, J. Opt. Soc. Am. A 9 (1992) 2159.
[22] T.D. Visser, S.H. Wiersma, J. Opt. Soc. Am. A 11 (1994) 599.
[23] C.J.R. Sheppard, P. Török, Bioimaging 5 (1997) 205.
[24] P. Török, P.D. Higdon, T. Wilson, J. Mod. Opt. 45 (1998) 1681.
[25] P. Török, P.D. Higdon, T. Wilson, Opt. Commun. 148 (1998) 300.
[26] P.D. Higdon, P. Török, T. Wilson, J. Microsc. (Oxford) 193 (1998) 127.
[27] P. Török, Opt. Lett. 25 (2000) 1463.